Performance evaluation of an airfoil under ice accretion using CFD simulations

Performance evaluation of an airfoil under ice accretion using CFD simulations

Daniel Bodenlle-Toral[1], Pedro García-Regodeseves[1], Adrián Pandal-Blanco[1]

[1] Department of Energy, University of Oviedo

garciarpedro@uniovi.es

Abstract. The profiles used in wind turbine blades have a great effect on aerodynamic behavior. The incorporation in engineering methods of the three-dimensional and rotation effects obtained through numerical simulations has allowed to substantially improve the design of the blades. A further advance in the improvement of the models is the modification of the surface state of the profile due to environmental effects. The presence of erosion, dirt, or snow on the leading edge reduces the aerodynamic behavior of the profiles. Therefore, incorporating its effects would improve predictions. However, the implementation of these effects in numerical models is complex. In this work, only the effect of the ice/snow accretion will be taken into account. The study is made using the NREL PHASE VI experimental horizontal-axis turbine with the S809 profile. The BEM theory is applied to conduct accurate 2D numerical simulations firstly, of a clean profile (unmodified) and afterwards of accreted profile. The latter is constructed by the modification of the profile in advance, following indications of the Icing ANSYS Fluent tool. Simulations are conducted under a RANS numerical approach through an SST k-ω model, which properly predicts boundary layer behavior. CFD results are evaluated at different sections of the profile and compared against predictions from other authors in terms of aerodynamic coefficients. The simulations consistently predict an increase in the drag coefficient (C_D +33%), and a decrease in the lift coefficient (C_L -9%). The presence of ice accretion affects the airfoil performance along the whole blade span, being slightly more pronounced towards the root of the blade. This work presents a new engineering methodology able to accurately predict airfoil performance under ice accretion at a reduced computational cost.

1. Introduction

Wind energy is one of the renewable sources with the highest installed and produced power in the world. It currently contributes approximately 20% of the electricity consumed. Its growth has been exponential since the beginning of the century. Not only has the number of wind farms been increased, but also studies to improve the performance of wind turbines [1].

The countries of northern Europe have a large percentage of wind energy, in many cases producing more than half of the electricity consumed. Weather conditions in these countries affect the operation of wind turbines. Among the causes stands out the accumulation of ice that causes a decrease in aerodynamic performance due to a change in the geometry of the blade, an increase in the static and dynamic loads to which the blade is subjected, and an acceleration in the fatigue of the material. Annual losses in 2010 due to ice accumulation are estimated to be around 20% of annual energy production [2].

Given that wind energy production occupies an increasing percentage of electricity generation, it is interesting to study the different behaviors depending on the accumulation of ice. These studies can be

carried out in laboratories where the blade is experimented on a reduced scale to analyze its behavior with the experimental data. However, wind tunnel testing is time-consuming and expensive. For this reason, CFD simulations are used as an alternative, which through numerical methods and algorithms try to predict the behavior of the air around the blade. By using CFD techniques, different types of geometries can be analyzed at a lower cost, and information is provided as a preliminary step to the experimental data obtained in the laboratory.

Fu and Farzaneh [2] investigated the accumulation of ice on a blade in 3D, the main findings were that most of the ice accumulates on the leading edge, and this accretion decreases as it approaches the base. Palacios [3] focused on investigating this ice accumulation with experimental tests, with which he obtained that the greatest accumulation occurs at the leading edge of the blade and that accumulation is greater if the angular velocity of the blade increases.

Concerning the accumulation of ice, Biancolini [4] investigated the variations that can be made on the mesh of the augmented profiles to optimize the workflow, and achieve quality results with less computational cost.

Hudecz et al. [1] analyzed the behavior of drag and lift coefficients in a wind tunnel and using CFD to contrast the results. They obtained similar results in both cases and concluded that due to the accumulation of ice the lift coefficient decreased, and the drag coefficient increased. This reduction in lift implies a loss in energy production. Also focused on the lift and drag coefficients, Kollár and Santos [5] investigated the variation of these coefficients as a function of ice accumulation, they concluded that after an hour and a half in freezing drizzle conditions the “lift to drag” ratio was half that in normal conditions and after two hours it was only one third, reducing production performance. It is also noted that the accumulation of ice depends substantially on the time the blade is subjected to these conditions, the longer the accumulation of ice will be.

The aim of the work is focused on analyzing the behavior of the coefficients of the "NREL Phase VI" wind turbine with the clean S809 profile and once the ice has been deposited on it. Studying the profile in different radial positions of the blade to observe the differences in behavior depending on the ice accumulated in each area

This study proposes a new methodology to predict the aerodynamic behavior of profiles augmented by ice, based on the combination of 2D simulations together with the BEM theory. And predict the shape of the ice in the profiles with the Icing Fluent tool to analyze the performance with those accumulations. To validate the method, the results of Fu and Farzaneh [2] are simulated.

2. Methodology

In this study, CFD techniques are used to determine the behavior of the flow around aerodynamic profiles. Although it has a higher computational cost, it is a widely used tool to try to predict the aerodynamic performance of wind turbine profiles.

2.1. NRELwind turbine model

The “NREL Phase VI” wind turbine [6] is a horizontal axis wind turbine. The geometry of the blade and the profile that it forms, the S809, are available in references [7] and [8]. Figure 2. shows the NREL turbine, the geometry of the blade, and the profile that forms it.

The profiles of the blade in different radial positions are analyzed to be able to compare the results of the ice accumulation with those shown by Fu and Farzaneh [2].

2.2. Simulation settings

The aerodynamic behavior of the “NREL Phase VI” blade has been studied in four radial positions: R= 2m (r/R = 0.361); R= 3m (r/R = 0.543); R= 4m (r/R = 0.723) and R= 5m (r/R = 0.904). Table 1. indicates the chord and the torsion angle (β) corresponding to the four radial positions.

Table 1. Radial position data along the blade.

r (m)	r/R	Chord (m)	Torsion (º)
2	0.361	0.661	7.559
3	0.543	0.56	1.676
4	0.723	0.459	-0.346
5	0.904	0.358	-1.775

Figure 1. shows the distribution of the chord and the torsion angle as a function of the radial position.

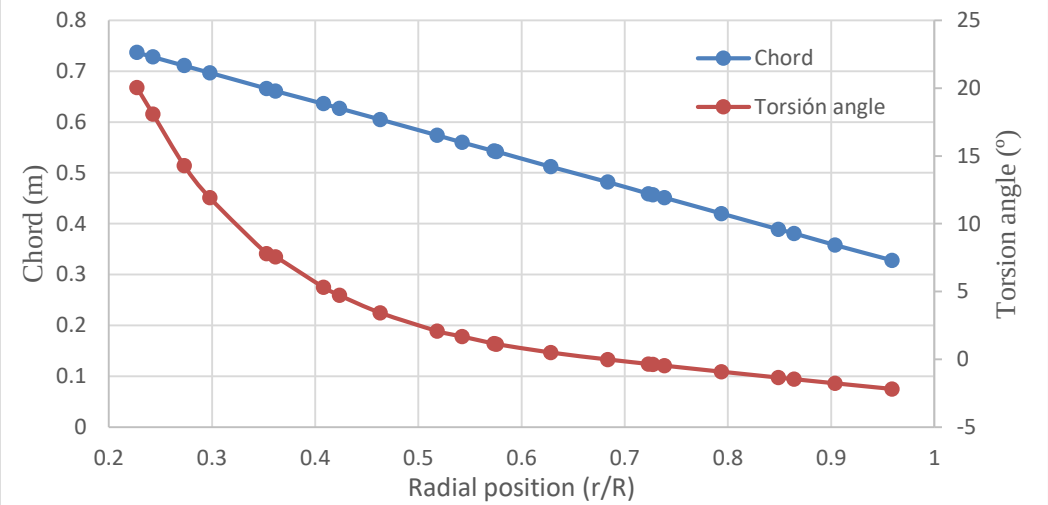

Figure 1. Chord size and twist angle as a function of radial position along the blade.

The conditions of the simulations have been 7 m / s of wind speed and 7.5 rad / s of rotation speed.

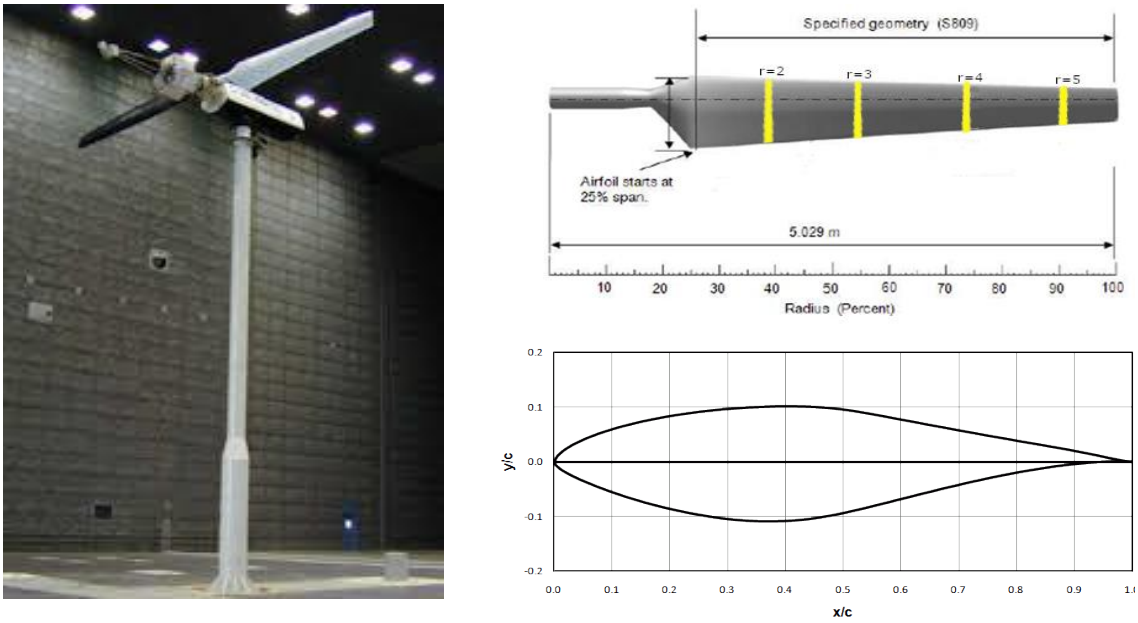

Figure 2. NREL Phase VI turbine (left), turbine blade (upper right) and S809 profile that forms the blade (lower right) [6].

2.3. Mathematical model

The simulations were carried out using the RANS equations (1) and (2) for incompressible flow with the SST *k-ω* (Shear-Stress Transport) turbulence model. Equation (1) indicates the conservation of mass and (2) indicates the conservation of moment. The governing equations were solved with the commercial code "Ansys Fluent" using the Finite Volume Method (FVM):

$$\frac{\partial \rho}{\partial t} + \nabla \cdot (\rho \cdot \vec{v}) = S_m \tag{1}$$

$$\frac{\partial}{\partial t}(\rho \cdot \vec{v}) + \nabla \cdot (\rho \cdot \vec{v} \cdot \vec{v}) = -\nabla p + \nabla \cdot (\vec{\tau}) + \rho \cdot \vec{g} + \vec{F} \tag{2}$$

Where ρ is the density of the fluid, t is time, $\vec{v}$ is the vector field of fluid velocity, p is pressure, $\vec{g}$ is gravity and $\vec{F}$ corresponds to other volumetric forces which for the case of this work are none. The term S_m that appears in (1) refers to the mass additions that occur from outside the system, in this case, there are none, then it will be 0, and the term $\vec{\tau}$ in (2) is the stress tensor.

The turbulence treatment complements the RANS equations to solve them, in this work the SST *k-ω* was used because it is a hybrid model that combines *k-ω* near the wall and *k-ε* in the outer part of the layer limit when the flow is fully turbulent, also features a modified turbulent viscosity formulation to account for main turbulent shear stress transport effects.

The selection of the turbulence model depends on the specific problem, no turbulence model is suitable for all conditions, therefore analysis is required to determine the best one in each case. This analysis is closely linked to the Y + parameter and the transition of the boundary layer near the walls

A study was conducted using the SST *k-ω* model and it was compared with the Realizable *k-ε* (RKE) model with Enhanced Wall Treatment (EWT). The simulations to compare both turbulence models were carried out on the NACA 2412 profile due to the availability of more bibliography to contrast the results [9]. It was obtained that the SST *k-ω* turbulence model improved the precision near the wall, in agreement with previous studies [10]. Therefore, this turbulence model was the one used for all simulations with the S809 profile.

The pressure-based algorithm was used to solve the RANS equations for incompressible flow. The coupling of pressure and velocity was solved by the SIMPLEC scheme

Regarding spatial discretization, second order schemes were used for pressure, moment, turbulent kinetic energy, and the specific dissipation rate. The gradient in each cell was determined with the "Green-Gauss Cell-Based" algorithm. The temporal discretization was stationary in all simulations, except those that simulated ice accumulation with "Icing".

2.4. Computational domain

The computational domain is the region of space where the behavior of the flow is studied. The choice of a good domain is essential since if it is too small it affects the normal development of the flow and if it is too large the computational cost increases too much. To determine the dimensions of the domain, a previous study of aerodynamic profiles with contrasted results was used [10].

The computational domain is a rectangle 21c long and 25c high whose input is a semicircle that closes the rectangle and that is 11.5c apart from the profile. Being c the chord of the profile. The size of the computational domain was chosen to ensure that there were no interferences between the boundary conditions and the flow around the profile. More than 10c was left from the entrance to the profile. And 21c with the outlet of the flow, so that the wake could develop normally. Regarding the height, 12.5c was left with the upper and lower entrance. The computational domain is shown in Figure 3.

2.5. Boundary conditions

The boundary conditions used were: (1) Velocity inlet in the semicircular line and in the upper and lower lines of the rectangle for the flow inlet; (2) non-slip wall in the profile and (3) pressure outlet for the flow outlet.

2.6. Meshing strategy

The information from previous studies for the S809 profile is scarcer than for other profiles For this reason the NACA 2412 was chosen to test and design a good mesh with contrasted results, and later transfer that mesh to S809 [11]. A structured mesh was generated manually throughout the domain, with special attention to the region near the profile walls to create an adequate boundary layer.

This mesh is transferred to the S809 profile, being necessary a small adaptation for the cells close to the profile walls.

The final mesh has 60060 cells. Figure 3. shows the mesh, the dimensions of the domain, and the boundary conditions, as well as a detailed view of the mesh in the areas close to the profile.

As for the augmented profiles, the same mesh was used, but adaptation was necessary for the front part where the geometry is modified by the ice. This adaptation consisted of a finer meshing in the areas where there were very sharp angles since the previous cells were not capable of adapting well to the geometry and precision was lost in the boundary layer.

For the boundary layer to better adapt to the profile, a division was made from a third of the chord so that the mesh could be straighter in the central area of the profile.

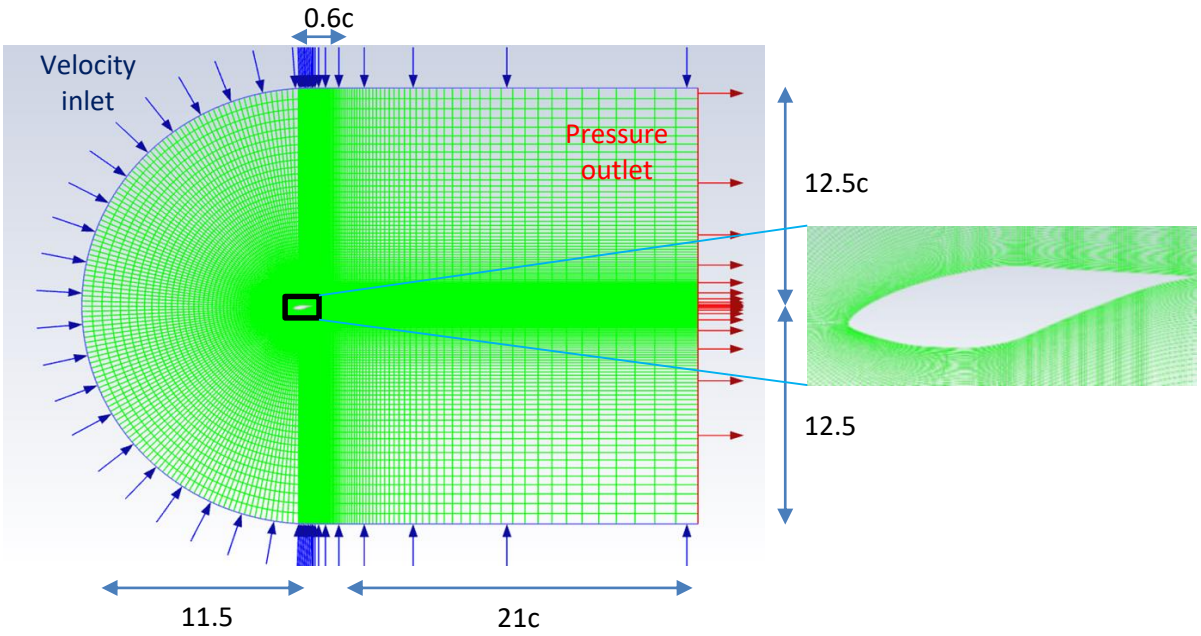

Figure 3. Dimensions of the computational domain and boundary conditions. Mesh in the areas close to the profile.

2.7. BEM Theory

The blade element moment theory (BEM) is widely used to predict the aerodynamic performance of horizontal axis wind turbines [12].

It is an iterative method to find the axial induction factor (a) and the tangential induction factor (a'). It consists of finding the angle of attack to obtain the aerodynamic coefficients (C_L and C_D), correcting the formulas with the Prandtl factor (F), and a and a' from (3) and (4) respectively:

$$a = \frac{1}{\frac{4 \cdot F \cdot \sin(\varphi)^{2}}{\sigma \cdot C_x} + 1} \tag{3}$$

$$a' = \frac{1}{\frac{4 \cdot F \cdot \sin(\varphi) \cdot \cos(\varphi)}{\sigma \cdot C_t} - 1} \tag{4}$$

For each iterative step, it is necessary to find C_L and C_D which vary depending on the Reynolds number and the angle of attack. These data to complete the BEM were extracted from [7].

Figure 4. shows a diagram with the velocity triangles in the rotor plane, the angles, and the forces generated in the profile.

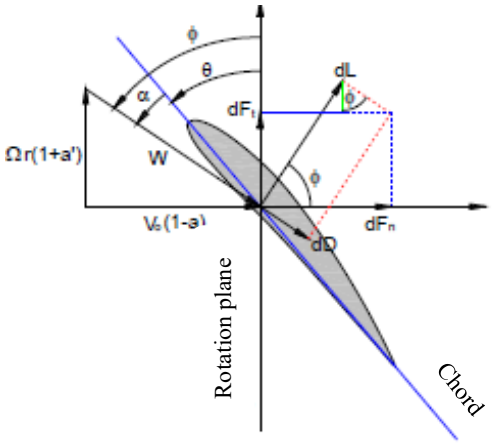

Figure 4. Components of the relative velocity in the rotor plane of a profile [13].

All the radial positions shown in [7] were calculated, in order to be able to analyze the variation throughout the entire blade.

Table 2. shows the axial and tangential induction factors and the angle of attack for each radial position.

To verify the results of the BEM method, they were compared with two previous studies. Induction factors were compared with [14], whereas the C_L and C_D values of each radial position were compared with [7].

Figure 5. shows the graph of the aerodynamic coefficients as a function of the angle of attack obtained with the BEM method. The equations for relating the coefficients to the forces are (5) and (6):

$$F_L = C_l \cdot 0.5 \cdot \rho \cdot V^2 \cdot A \tag{5}$$

$$F_D = C_d \cdot 0.5 \cdot \rho \cdot V^2 \cdot A \tag{6}$$

Where F_L is the lift force and F_D is the drag force, ρ is the air density, V is the relative wind speed (m/s), A is the area of the profile that at being 2D is the chord (unit thickness) and φ is the inflow angle.

Table 2. Results of the BEM method according to the position. The angle of attack, the axial and tangential induction factors are indicated.

r/R	AoA (º)	a	a'
0.227	7.841	0.14471	0.06191
0.243	8.205	0.14851	0.05538
0.273	9.202	0.15708	0.04524
0.298	9.694	0.16051	0.03832
0.353	9.876	0.18637	0.03101
0.362	9.718	0.18501	0.02946
0.408	9.820	0.18975	0.02343
0.424	9.793	0.19081	0.02180
0.463	9.659	0.19393	0.01842
0.518	9.342	0.19807	0.01496
0.542	9.109	0.20029	0.01410
0.573	8.890	0.20284	0.01278
0.576	8.869	0.20315	0.01269
0.628	8.409	0.20642	0.01091
0.683	7.939	0.21070	0.00948
0.723	7.677	0.21213	0.00851
0.727	7.649	0.21257	0.00842
0.739	7.577	0.21361	0.00819
0.794	7.264	0.22024	0.00725
0.849	6.956	0.23364	0.00662
0.864	6.859	0.23968	0.00652
0.904	6.571	0.26188	0.00638
0.959	5.808	0.33612	0.00691

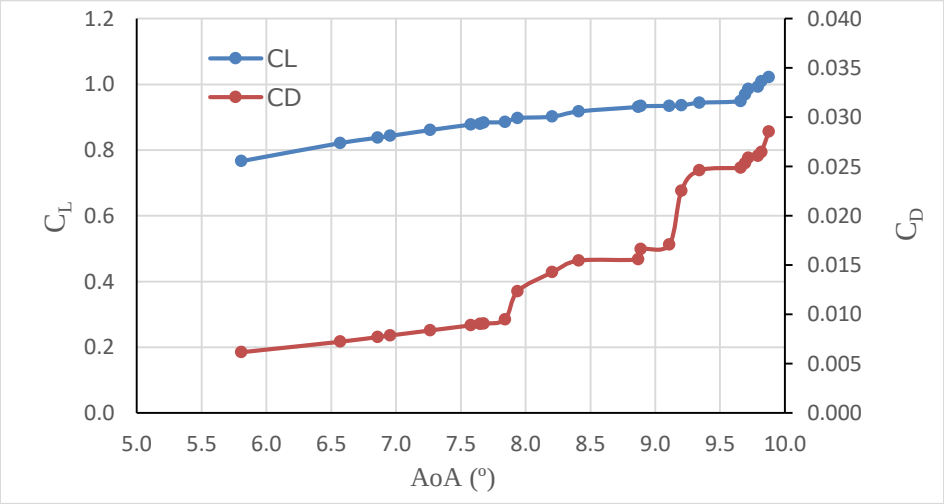

Figure 5. Aerodynamic coefficients as a function of the angle of attack obtained with the BEM method.

2.8. Icing Fluent

ANSYS Fluent Icing tool was used to predict the accumulation of ice and obtain the way it adheres to the profile.

It is based on the results of the flow around the clean profile as a base and the "Icing" predicts the behavior of the droplets on the profile and the accumulation of ice.

For the droplets the “Monodispersed distribution” and “Langmuir-D Distribution” models are the most used, they differ in the way of calculating the distribution of the drops along with the profile. It was found that the “Monodispersed distribution” model provided good results without excessive calculation time.

Regarding the accumulation of ice, the two available software are “Fluent Icing Ice Accretion” and “Multi-shot Ice accretion”. The second is specialized for more complex geometries and is based on the displacement of the mesh, which substantially increases the calculation time. For the case of this work, the first one provides enough precision to predict the accumulation of ice in the profiles.

Within the software of "Fluent Icing Ice Accretion" there are several models to simulate ice accumulation, the two most used are "Glaze" and "Rime". The “Rime” Model is more focused on the formation of the ice at the beginning while the “Glaze” Model is more focused on the accumulation once the ice has already formed. After analyzing the results, "Glaze" is chosen for presenting greater precision for the conditions of this work.

3. Results and Discussion

Simulations of the clean profile and the augmented profile found with "Icing" were carried out for the four radial positions indicated in order to analyze the differences in the velocity and pressure contours. In addition, the aerodynamic coefficients (C_L and C_D) and the pressure coefficient (C_P) along the profile were obtained to verify the results.

The ice contours found with "Icing" are compared with the results of Fu and Farzaneh [2]. For this reason, simulations of their augmented profiles were also carried out.

3.1. Clean profiles

Figure 6. shows the contours of velocity (left) and pressure (right) for each of the radial positions with the clean profiles.

At the upper part of the leading edge, the streamlines of the flow come together due to the inclination of the angle of attack, which produces an increase in velocity and a decrease in pressure, because the total pressure must remain constant, then if dynamic pressure increases, static pressure decreases. After passing the first half of the upper surface the streamlines are separated by the geometry of the profile, which produces a decrease in speed and the recovery of pressure to atmospheric pressure that is maintained until the end of the profile. The velocity decreases in the profile because the streamlines are not able to follow the curve in the geometry and separate from the profile.

At the lower part of the leading edge, the so-called stagnation point is formed. As it moves along the lower surface, the speed recovers because the streamlines come together again until the local maximum

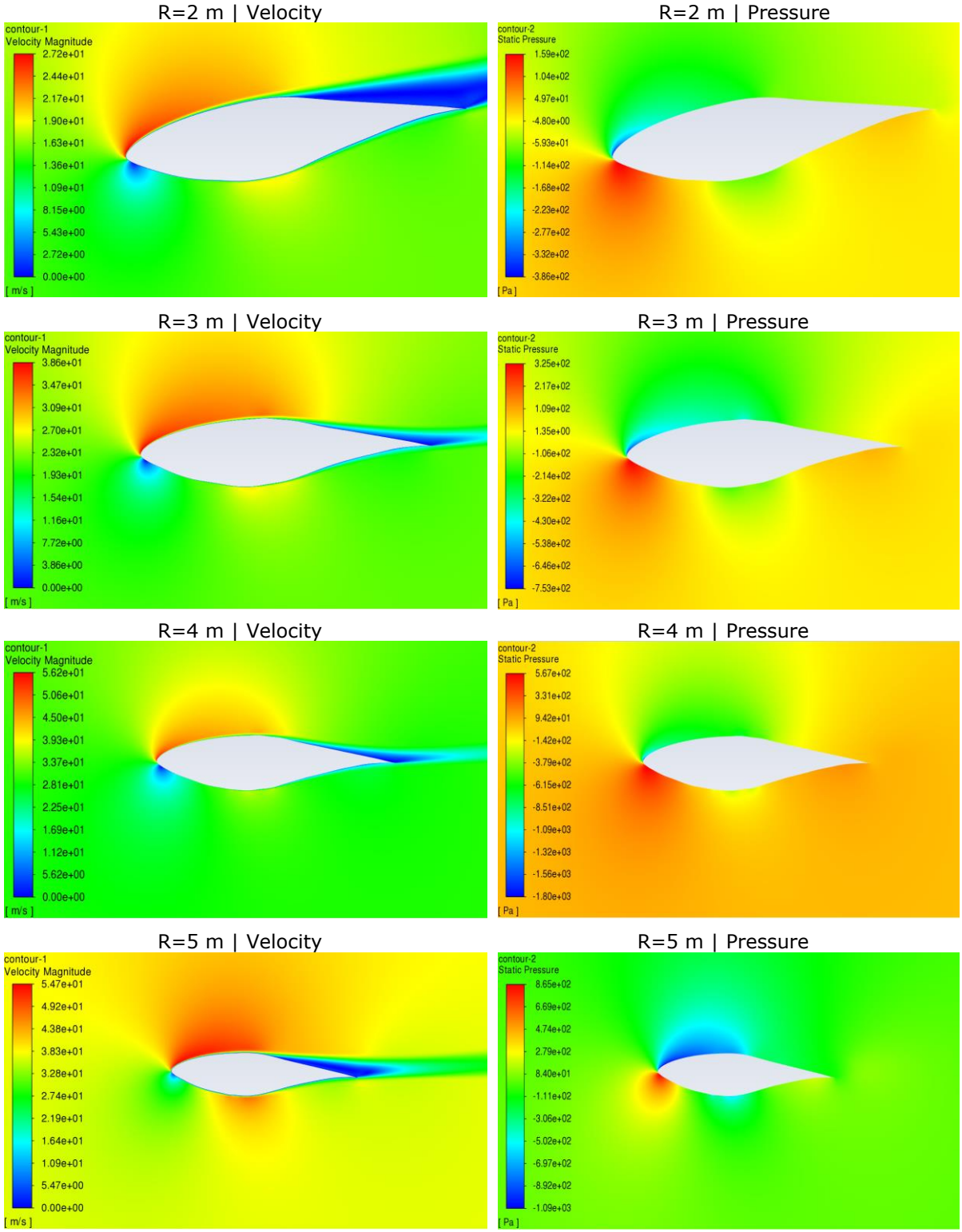

Figure 6. Contours of velocity (left) and pressure (right) of the clean profiles.

speed is reached in the middle, which coincides with the curve of the profile, where there is a depression. From this point, the speed decreases, which causes the pressure to recover to atmospheric and remain until the trailing edge.

3.2. "Icing" profiles

After studying the behavior of the flow around the clean profiles, the accumulation of ice is analyzed. To do this, the accretion of ice in the profile is simulated sing "Fluent Icing" and then the behavior of the flow around these profiles with ice is analyzed.

To carry out the simulations of the "Icing" the conditions are extracted from the study of Fu and Farzaneh [2]. Air temperature -10ºC; Liquid Water Content (LWC) 1 g/m^3; Medium Volumetric Diameter (MVD) of the droplet 20 µm, ice density 300 Kg/m^3 and the roughness of the profile wall 0.0005 m.

It should be noted that despite using the same conditions, Fu and Farzaneh [2] simulate ice accumulation with their equations. While in this work the dispersion of the drops is simulated with the "Monodispersed calculation" model and the accumulation of ice with "Fluent Icing Ice Accretion" with the "Glaze" model.

The "Fluent Icing" function is only valid for 3D meshes, that is why all the profiles have been extruded 0.1 m.

When simulating the accumulation of ice, time is a key parameter since the accumulated volume depends on it. To observe the variation with time, three cases have been simulated: 400 s, 900 s, and 2000 s. Figure 7. shows the 2D contours of the profiles with the ice accumulations at the three indicated times.

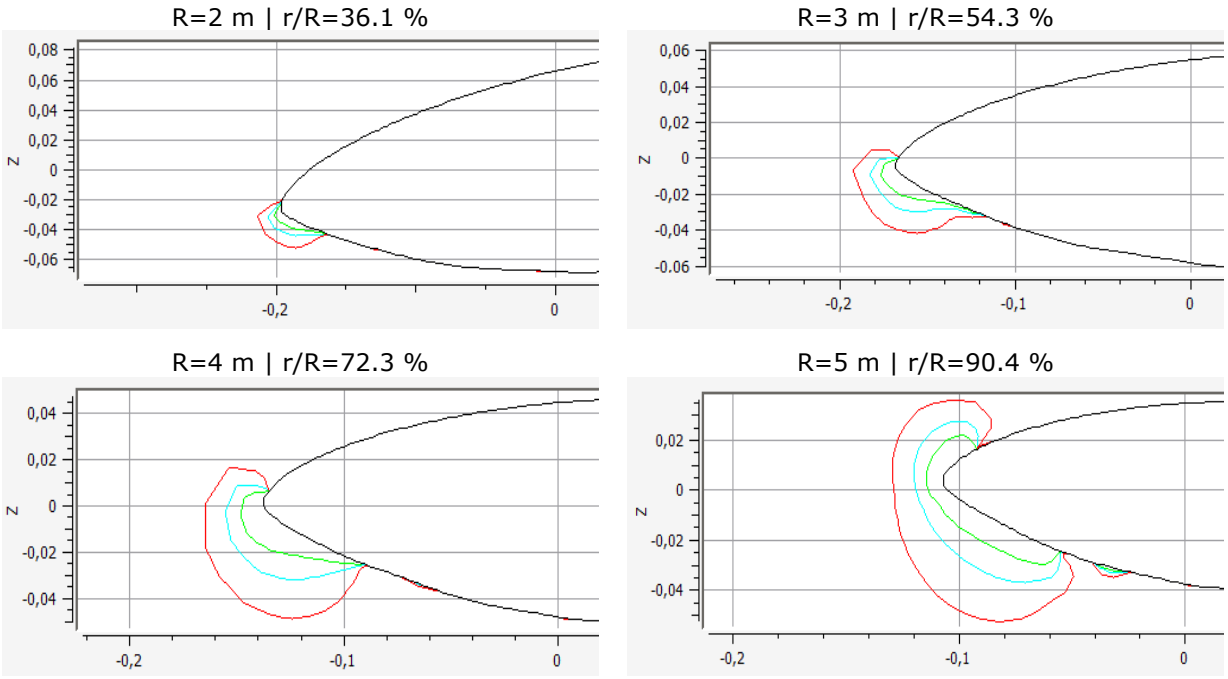

Figure 7. Ice accumulations on the profile for 400 sg (Green), 900 sg (Blue), and 2000 sg (Red).

The radial positions close to the base have less ice accumulation than the distant ones, that is why the amount of ice accumulated is less at r = 2 m and as it moves away from the base it goes growing until r= 5 m which is where the greatest accumulation occurs.

Within the shape of the ice contours, accumulation is created at the bottom of the leading edge. This accumulation increases as it gets closer to the tip of the blade and occupies a greater area of the lower part. Regarding time, as the simulation time increases, the amount of ice deposited increases.

Once the profiles with ice accretion were obtained with "Icing", they were simulated to be able to compare the results with the clean profiles and contrast them with the results of the augmented profiles. For this, 2D meshes were created again from the contours of the "Icing".

Figure 8. shows the contours of velocity (left) and pressure (right) for each of the radial positions with the augmented profiles obtained with "Icing".

As one advances towards the tip the accumulation of ice is greater, therefore, the greatest differences are found at r= 5 m, and the smallest at r= 2 m. It is important to note that there is less difference in geometry due to the ice near the base, but in this area, the angle of attack is greater so the variations in the dimensionless coefficients are greater. Although the ice accumulations are different, the same conclusions can be drawn from all the profiles.

What stands out the most is that there is an accumulation point in the upper part where the speed is maximum and the pressure is minimum, making the speed after that point on the upper surface not as great as in cases without ice. As for the lower part, the shape of the ice creates zones of zero velocity, which creates several points of stagnation.

Because there is less pressure jump because the depression in the upper surface is not so small, the lift force will be less, then a decrease in the C_L is expected.

As for drag, the ice supposes a modification in the geometry and makes the leading edge larger, which increases the drag because there is more friction with the air. Then an increase in C_D is expected.

3.3. Augmented profiles

The results of ice accumulation with "Icing" are compared with the previous study by Fu and Farzaneh [2]. Figure 9. shows the contours of velocity (left) and pressure (right) for each of the radial positions with the augmented profiles.

The accumulation of the ice coincides with the "Icing" because as it approaches the tip of the blade the accumulation is greater. But the contour of this accumulation is different, possibly due to changes in methodology. Fu and Farzaneh used their equations and the k-ε turbulence model, while in this work the “Icing” model of “Fluent” and the SST *k-ω* turbulence model were used. The accretions they got are very horizontal and build up from the front of the leading edge with very sharp corners, while the builds for this study start at the leading edge but gather more towards the bottom along with the profile.

The general shape of the contours is like the case of “Icing”, in the upper surface there is a decrease in pressure due to an increase in speed, and in the lower surface, there is an increase in pressure due to the slowing down.

Due to the presence of ice on the leading edge, the point where the speed is maximum and the zero pressure is transferred to the upper tip of the ice, which modifies the depression that occurs in the upper surface, behavior like the case of the profiles increased.

As a result of this accumulation of ice, a stagnation zone is produced at the beginning of the lower surface since the current lines do not reach that zone and the pressure is maximum.

Because of the changes in the pressure gradient, a decrease in C_L is expected, since bearing force is lost due to the change in pressures in the upper surface in reference to the clean profiles. And due to the modification of the geometry of the leading edge, an increase in the C_D is expected because it presents a greater drag than the clean profiles.

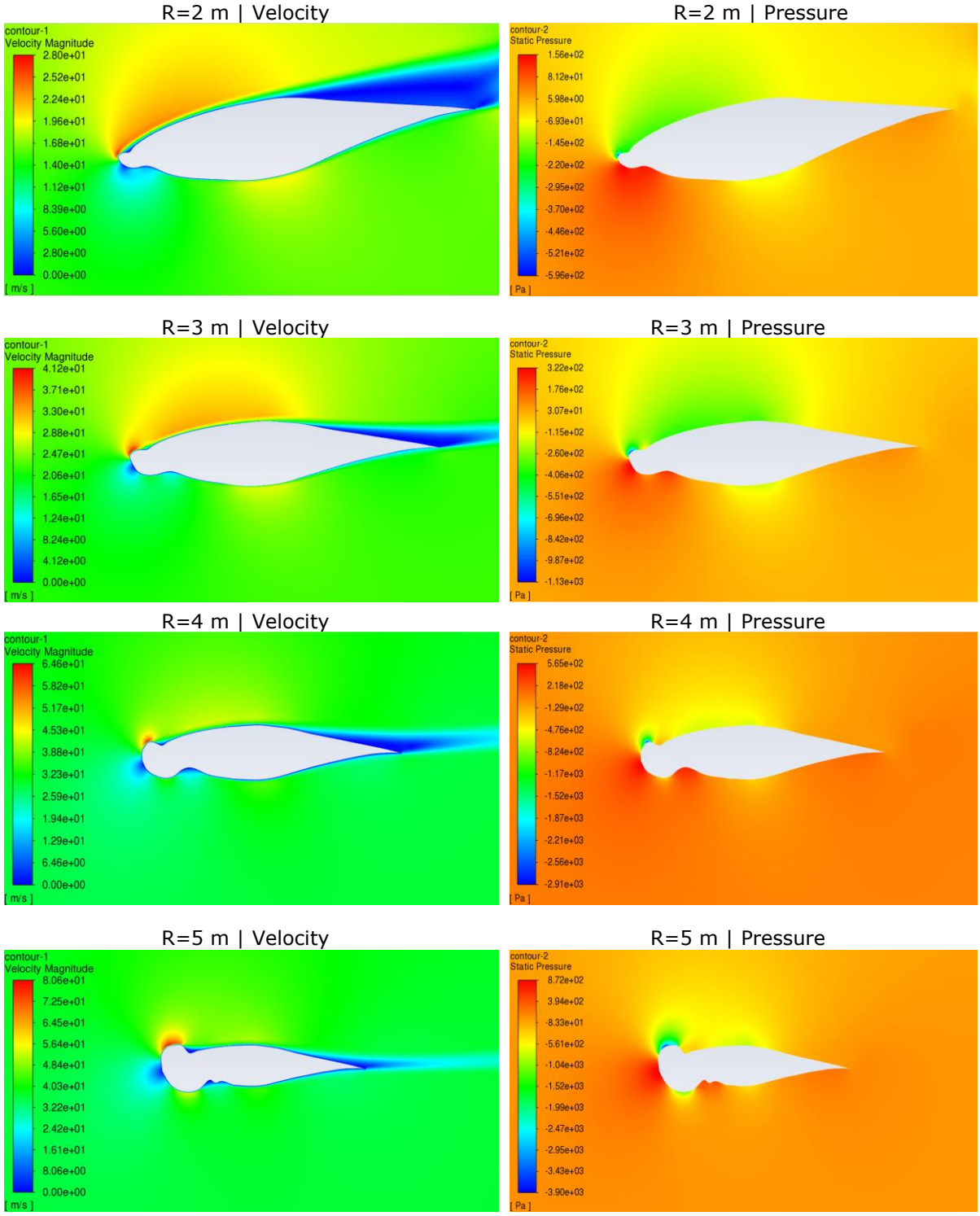

Figure 8. Contours of velocity (left) and pressure (right) of the profiles with "Icing".

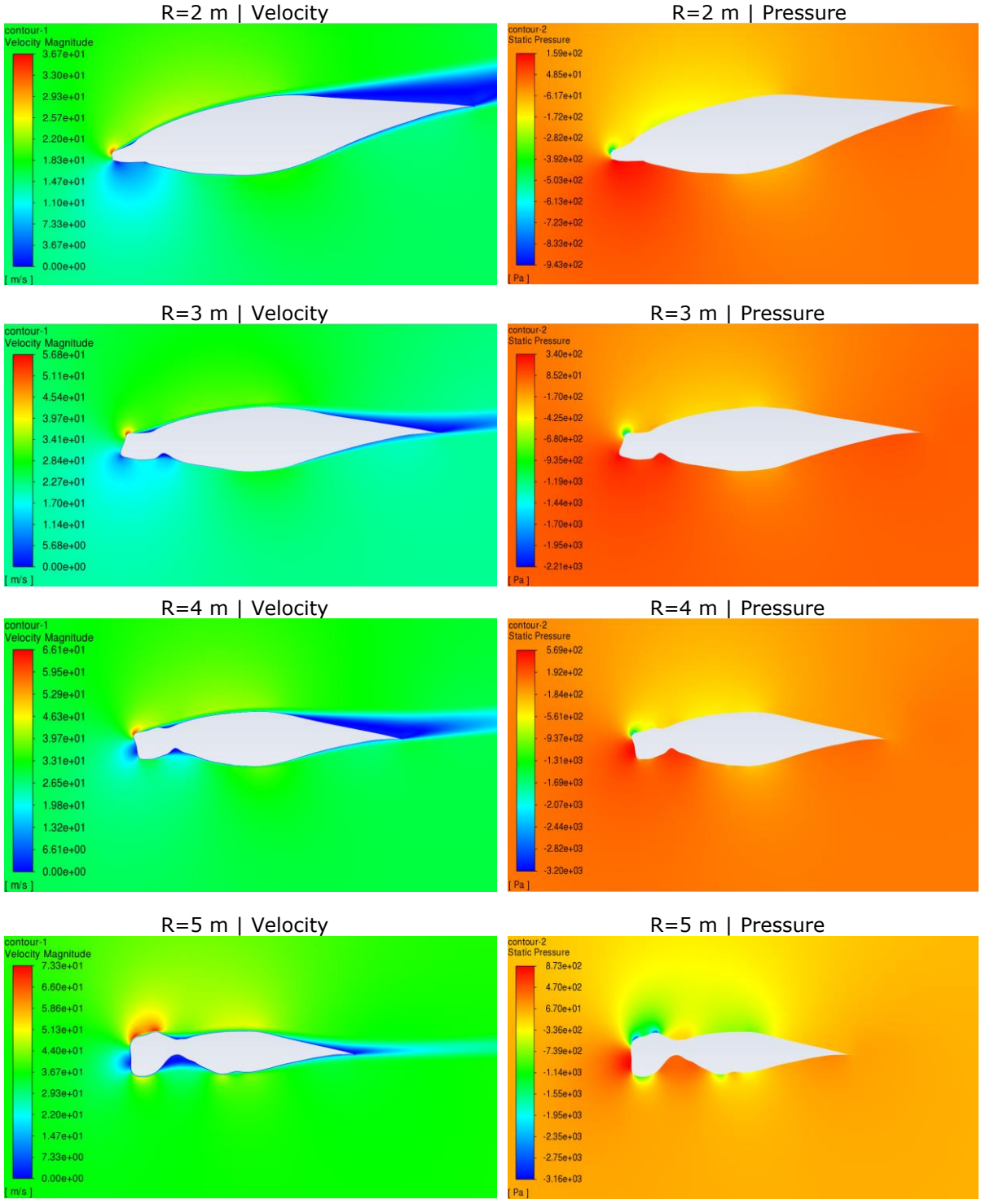

Figure 9. Contours of velocity (left) and pressure (right) of the augmented profiles**.**

Figure 10. shows the pressure coefficients (C_P) along the profiles in the four radial positions for the three simulated cases. They have similar behavior in the three cases, but the profiles with "Icing" (Red) and increased [2] (Green) have a greater variation in the front part with respect to the clean profile (Blue). This is due to ice, which accumulates mainly at the leading edge and changes pressure distributions. The C_P is determined at all the points of the profile for each of the cases according to equation (7):

$$C_p = \frac{P - P_\infty}{0.5 \cdot \rho \cdot V^2} \tag{7}$$

Where P is the pressure of the profile, P_∞ is the pressure at the domain inlet (similar to the atmospheric), ρ is the density of the air and V is the velocity of the air in each case.

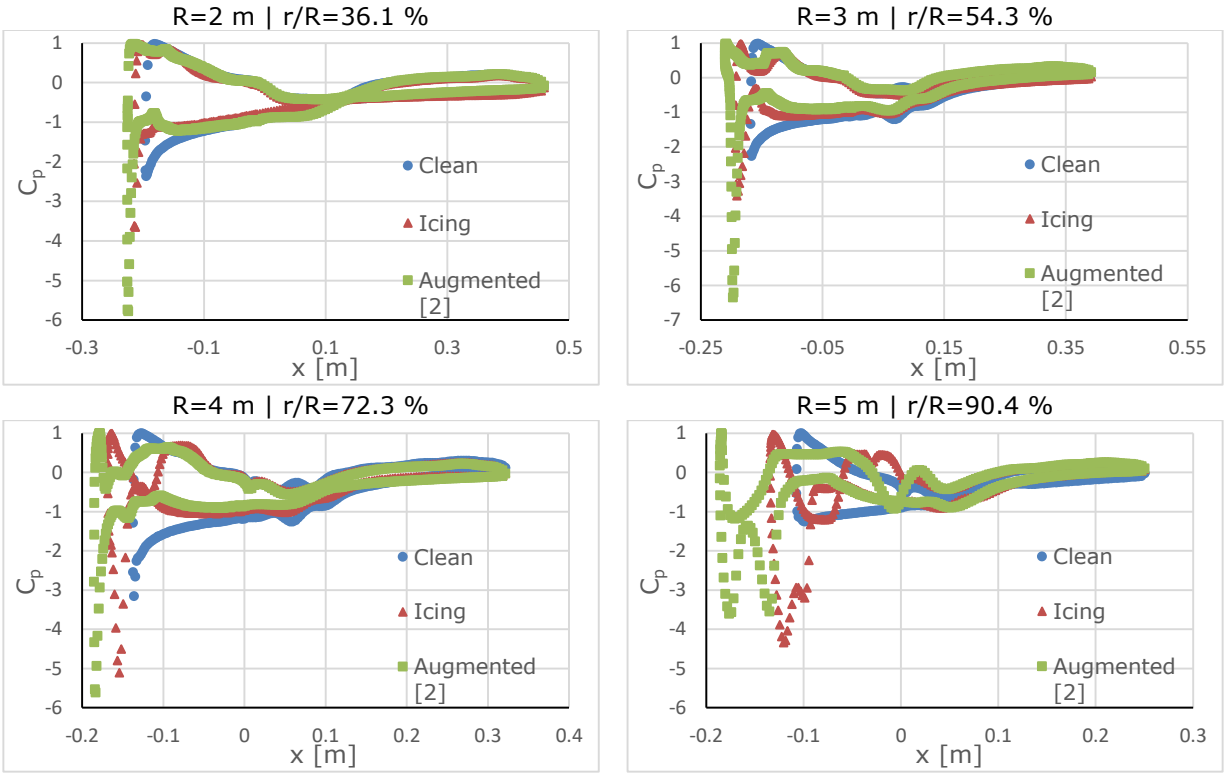

Figure 10. Pressure coefficients along with the profiles in the different radial positions.

3.4. Comparison C_L and C_D

After having compared the contours of the clean profiles and the profiles found with "Icing", the lift coefficient C_L and the drag coefficient C_D are compared.

In this work, results of these coefficients were obtained with: the BEM theory according to the data of [7]; the clean profiles; the profiles with "Icing" and the augmented profiles of [2].

The coefficients have the expected behavior, both C_L and C_D increase as the angle of attack increases and the detachment zone is not reached where the C_L drops drastically, which for this profile is around 15º. The critical angle varies based on the Reynolds as shown in [15] y [16].

Figure 11. shows the comparison of the C_L and Figure 12 shows the comparison of the C_D. The results of the clean profiles (Blue) are very similar to those of the BEM theory (Green), in such a way that the procedure to find the coefficients and the contours of the clean profiles can be verified. And the results of the profiles with "Icing" (Purple) and augmented (Red) are very similar and present the expected behavior indicated by the contours. The C_L decreases because there is a lower pressure difference between the lower and the upper surface, and the C_D increases due to the profile exhibit more drag due

to the change in the front-end geometry. The changes with the "Icing" profiles are a little less because the shape of the ice accumulation is not as pronounced as that of the increased profiles and follows the line of the profile more uniformly.

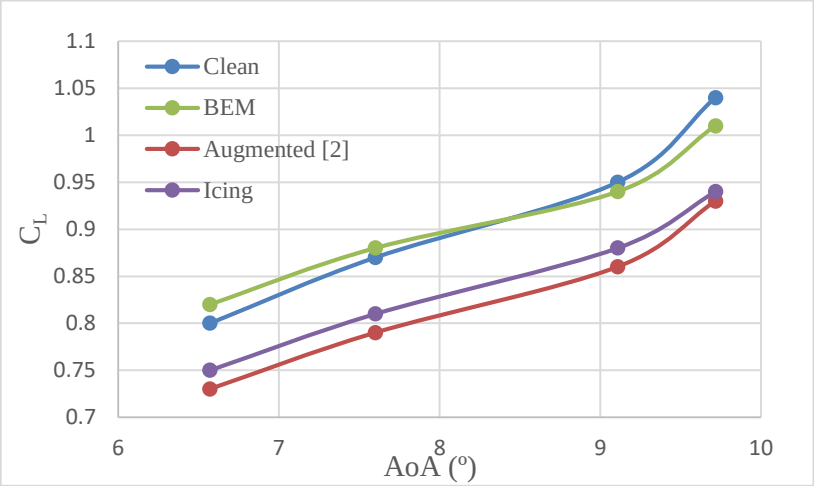

Figure 11. Comparison of the C_L according to the angle of attack.

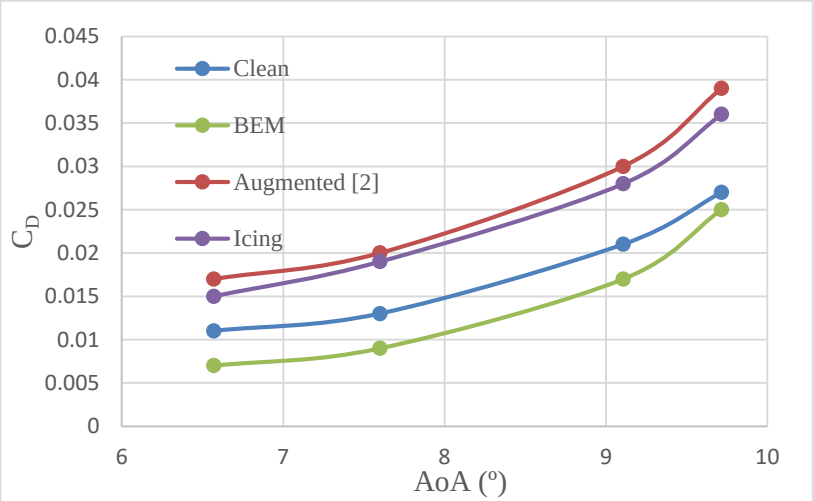

Figure 12. Comparison of the C_D according to the angle of attack.

Comparing the differences of the clean profiles with the profiles obtained with "Icing" it can be extracted that the C_L decreases around 9% and that the C_D increases by 33% due to the presence of the ice. These percentages are very similar in all radial positions, although near the base the differences are slightly higher since the angle of attack is greater.

4. Conclusions

The horizontal axis turbine blade "NREL PHASE VI" has been modeled in different radial positions (R= 2 m r/R= 0.361; R= 3 m r/R= 0.543; R= 4 m r/R= 0.723; R= 5 m r/R= 0.904) to study the aerodynamic behavior of their profiles. This aerodynamic behavior has been simulated under normal conditions and after ice accretion. The simulations have been carried out with the RANS equations complemented with the SST k-ω turbulence model. Apart from this mathematical model, the BEM method was used to increase the precision of the results, and the “Fluent Icing” tool to predict the accumulation of ice on the profile.

A complete validation of the numerical model was carried out. For this, simulations of the clean profile were carried out, supplemented with the BEM method to correct the speed, and take into account the effects of the rotation of the blades. Their results were compared with previous experimental data from [7] and [14] to confirm the methodology used.

After verifying the method with clean profiles, the accumulation of ice along the blade is studied using the "Icing" tool. The ice accretions in the different radial positions are obtained by varying the time of the simulations to observe the differences between them. Simulation time is determined to be a key parameter in determining ice accumulation.

Once the augmented profiles are obtained, they are modeled to simulate them and study the aerodynamic performance once the ice has accumulated. The same mathematical model used for the clean profiles was used for these augmented profiles. To validate the results of the augmented profiles, they were compared with the data obtained in [2].

Analyzing the results, it can be determined that due to the accretion of the ice there is a modification in the aerodynamic performance of the profiles, with an increase in the drag coefficient (C_D = + 33%) and a decrease in the lift coefficient (C_L = - 9%). These variations fluctuate slightly depending on the position of the blade being greater near the base.

References

[1] Hudecz A, Koss H and Hansen M O L 2013 Ice Accretion on Wind Turbine Blades 9
[2] Fu P and Farzaneh M 2010 A CFD approach for modeling the rime-ice accretion process on a horizontal-axis wind turbine *J. Wind Eng. Ind. Aerodyn.* **98** 181–8
[3] Palacios D J L 2010 Task A-1.13: Experimental Measurement of Ice Accretion and Shedding of Rotating Airfoils 37
[4] Biancolini M 2013 An Efficient Approach to Simulating Ice Accretion on 2D 6
[5] Kollár L E and Santos F O S 2019 Consideration of Icing in the Design of Wind Turbine Blade Sections 6
[6] Anon NREL Phase VI
[7] Hand M M, Simms D A, Fingersh L J, Jager D W, Cotrell J R, Schreck S and Larwood S M 2001 *Unsteady Aerodynamics Experiment Phase VI: Wind Tunnel Test Configurations and Available Data Campaigns*
[8] Anon Airfoil Tools, S809
[9] Oukassou K, Mouhsine S E, Hajjaji A E and Kharbouch B 2019 Comparison of the power, lift and drag coefficients of wind turbine blade from aerodynamics characteristics of Naca0012 and Naca2412 *Procedia Manuf.* **32** 983–90
[10] Anon 2019 Research onFlows for NACA 2412 Airfoil using Computational Fluid Dynamics Method *Int. J. Eng. Adv. Technol.* **9** 5450–6
[11] Wang Q, Yi X, Liu Y, Ren J, Li W, Wang Q and Lai Q 2020 Simulation and analysis of wind turbine ice accretion under yaw condition via an Improved Multi-Shot Icing Computational Model *Renew. Energy* **162** 1854–73
[12] Mourits J BEM theory and CFD for Wind Turbine Aerodynamics 73
[13] Fernández C C and Morros C S Diseño Aerodinámico Optimizado de un Aerogenerador de Eje Horizontal 16
[14] Yang H 2014 Prediction of the wind turbine performance by using BEM with airfoil data extracted from CFD *Renew. Energy* 9
[15] Zhu C, Qiu Y and Wang T 2021 Dynamic stall of the wind turbine airfoil and blade undergoing pitch oscillations: A comparative study *Energy* **222** 120004
[16] Gharali K and Johnson D A 2012 Numerical modeling of an S809 airfoil under dynamic stall, erosion and high reduced frequencies *Appl. Energy* **93** 45–52